International Journal of Pharmaceutics 635 (2023) 122780

Contents lists available at ScienceDirect

International Journal of Pharmaceutics

journal homepage: www.elsevier.com/locate/ijpharm

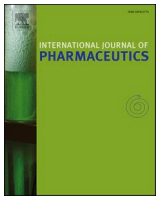

Selective laser sintering additive manufacturing of dosage forms: Effect of powder formulation and process parameters on the physical properties of printed tablets

Evgenii Tikhomirov [a], Michelle Åhlén [a], Nicole Di Gallo [b], Maria Strømme [a], Thomas Kipping [b], Julian Quodbach [c,*], Jonas Lindh [a,*]

[a] Division of Nanotechnology and Functional Materials, Department of Materials Science and Engineering, Ångström Laboratory, Uppsala University, Uppsala SE-751 03, Box 35, Sweden
[b] Merck KGaA, Frankfurter Str. 250, Postcode: D033/001, Darmstadt DE-642 93, Germany
[c] Department of Pharmaceutics, Utrecht Institute for Pharmaceutical Sciences, Utrecht University, Universiteitsweg 99, 3584 CG Utrecht, the Netherlands

ARTICLE INFO

Keywords:
Additive manufacturing
Three-dimensional printing
Selective laser sintering
Personalized medicines
Drug manufacturing

ABSTRACT

Large batches of placebo and drug-loaded solid dosage forms were successfully fabricated using selective laser sintering (SLS) 3D printing in this study. The tablet batches were prepared using either copovidone (N-vinyl-2-pyrrolidone and vinyl acetate, PVP/VA) or polyvinyl alcohol (PVA) and activated carbon (AC) as radiation absorbent, which was added to improve the sintering of the polymer. The physical properties of the dosage forms were evaluated at different pigment concentrations (i.e., 0.5 and 1.0 wt%) and at different laser energy inputs. The mass, hardness, and friability of the tablets were found to be tunable and structures with greater mass and mechanical strength were obtained with increasing carbon concentration and energy input. Amorphization of the active pharmaceutical ingredient in the drug-loaded batches, containing 10 wt% naproxen and 1 wt% AC, was achieved *in-situ* during printing. Thus, amorphous solid dispersions were prepared in a single-step process and produced tablets with mass losses below 1 wt%. These findings show how the properties of dosage forms can be tuned by careful selection of the process parameters and the powder formulation. SLS 3D printing can therefore be considered to be an interesting and promising technique for the fabrication of personalized medicines.

1. Introduction

Conventional drug formulations for oral administration are limited to only a few available dosage forms. Manipulations of such dosage forms are often carried out when treating particular patient groups with diverse and specific needs, e.g., pediatric patients (Kader et al., 2021; van der Vossen et al., 2019). According to two independent studies carried out in Sweden and the Netherlands, drug manipulations occurred in 15% (Kader et al., 2021) to 60% (van der Vossen et al., 2019) of cases in hospitals, depending on the age group and diagnoses of the patients. The most vulnerable patients were found to be toddlers and pre-school children, who require small dosage forms, which were typically prepared from commercially available pharmaceutical preparations as a slurry. However, only 41% of these medicines were prepared and manipulated according to the Summary of Product Characteristics (SmPc) or Package Information Leaflet (PIL) requirements (van der Vossen et al., 2019). This may lead to inaccurate dosing and such incorrect treatment could pose a serious risk in the remaining 59% of cases when these requirements were not followed. This demonstrates that the administration of oral medicines remains an issue not only for pediatrics but also for the treatment of other heterogeneous patient groups such as geriatric patients (El Aita et al., 2020; Trenfield et al., 2018; Charoo et al., 2020). Where the uses of off-label medications often lead to inefficient treatment due to differences between the pharmacogenetic and pharmacokinetic characteristics of these individuals and the general adult population (Trenfield et al., 2018; Konta et al., 2017). 3-dimensional printing (3D printing), however, has emerged during the last decade as a promising technique for the fabrication of personalized dosage forms. Structures of great complexity and intricacy, prepared using computer-aided design (CAD) software, have been obtained from various layer-by-layer deposition methods with relative ease (Trenfield et al., 2018). As such, the technique could prove useful for

* Corresponding authors.
E-mail addresses: j.h.j.quodbach@uu.nl (J. Quodbach), Jonas.Lindh@angstrom.uu.se (J. Lindh).

https://doi.org/10.1016/j.ijpharm.2023.122780
Received 5 December 2022; Received in revised form 20 February 2023; Accepted 22 February 2023
Available online 26 February 2023

manufacturing dosage forms with bespoke properties (i.e., geometries, drug release profiles, and appearances) on-demand and locally at hospitals according to each patient's needs (Seoane-Viano et al., 2021). Various 3D printing technologies have been investigated for the printing of medicines, including fused-deposition modeling (FDM) (Cailleaux et al., 2021; Gultekin et al., 2019; Kollamaram et al., 2018), binder jetting (Sen et al., 2021; Chang et al., 2020), stereolithography (SLA) (Healy et al., 2019; Martinez et al., 2018; Wang et al., 2016), and selective laser sintering (SLS) (Fina et al., 2018; Gueche et al., 2021; Fina et al., 2018; Fina et al., 2017), to name a few. In particular, the SLS technique may offer certain advantages, as compared to other 3D printing techniques, for the manufacturing of larger batches of dosage forms (e.g., 30 or 100 tablets per print) due to the instrument's large print volume and high packing density. The technique utilizes a laser beam at a certain wavelength as a source of energy to selectively fuse powder particles on the surface of a powder bed. Depending on the desired power and optical properties of the initial powder formulation the laser type may vary from laser diodes to CO_2-lasers (Gueche et al., 2021). The 3D structures are further constructed through the fusion and attachment of the sintered layers to each other and are stabilized in the build volume by the surrounding un-sintered powder. The SLS technique, therefore, does not require the use of additional supports which are typically required in FDM or SLA printing. Absorbing pigments, in the form of e.g. active carbons or iron oxide, are usually needed to enhance the sintering of the powders if the wavelength of the laser is in the IR- or Vis-region (Charoo et al., 2020; Fina et al., 2017; Schmid, 2018; Awad et al., 2020; Awad et al., 2021). The formation of amorphous solid dispersions (ASDs) from various active pharmaceutical ingredients (APIs) and polymers has also been demonstrated through SLS printing (Santitewagun et al., 2022; Trenfield et al., 2020; Madžarević et al., 2021; Trenfield et al., 2022). Thus, this shows that the technique may be promising for the manufacturing of dosage forms containing biopharmaceutical (BCS) class II or IV poorly water-soluble drugs (Thakkar et al., 2021; Davis et al., 2021; Hamed et al., 2021).

In this study, we present the fabrication of batches of 30 tablets of PVP/VA and PVA-based placebo and naproxen-loaded tablets using selective laser sintering 3D printing. The physical properties of the printed tablets, as a function of pigment concentration and laser energy input, were evaluated using powder X-ray diffraction and differential scanning calorimetry. A thorough analysis of the dimensions, weights, and friability of the tablets was carried out. The correlation between tablet hardness and printing-angle was further studied in order to investigate the anisotropy of the printed structures.

2. Materials and methods

2.1. Materials

Activated carbon (powder, mesh size 100, which corresponds to particles that passed through a sieve of 149 μm) was purchased from Sigma-Aldrich, USA. PVP/VA (Plasdone S-630, 60:40 linear copolymer of N-vinyl-2-pyrrolidone and vinyl acetate) was kindly provided by Ashland Industries Deutschland GmbH (Düsseldorf, Germany), and PVA (Parteck® MXP, polyvinyl alcohol, PVA), Aerosil (highly dispersed colloidal silica, SiO_2), and Naproxen manufactured by Fagron (Rotterdam, Netherlands) were generously provided by the Merck Group (Darmstadt, Germany).

All chemicals were used as received without further processing.

2.2. Powder preparation

Placebo and naproxen-loaded powder formulations were prepared according to Table 1. The compound names consist of three or five letters in the beginning which corresponds to selected polymer (i.e., PVP/VA or PVA) and the presence of the API (N – Naproxen). The second part of the name is the digit (0.5 or 1) which defined the AC weight percentage. All powder mixtures were sieved using a 315 μm stainless-steel test sieve (VWR International AB, Sweden) and mixed using a Turbula shaker (Turbula T2F shaker, Glen Mills, Inc., Clifton, NJ, US) for 15 min. AC and fumed silica were added to the formulations in order to enhance the laser energy absorption of the powders and to improve powder flowability during the printing process, respectively. The formulations were prepared in large enough batches (>1000 mL) to partially fill the build volume (150 × 200 × 150 mm).

Table 1
Composition of the prepared powder formulations used in this study.

Compound	PVA-05 (wt %)	PVA-1 (wt %)	PVA-N-1 (wt%)	PVP/VA-05 (wt%)	PVP/VA-1 (wt%)	PVP/VA-N-1 (wt%)
PVA	99	98.5	88	–	–	–
PVP/VA	–	–	–	98.5	98	88
AC	0.5	1	1	0.5	1	1
Aerosil (fumed silica)	0.5	0.5	1	1	1	1
Naproxen	–	–	10	–	–	10

2.3. Selective laser sintering 3D printing of dosage forms

Tablet models (Fig. 1) were created and designed in Solidworks 2019 SP05 (Dassault Systèmes Corporation, Vélizy-Villacoublay, France), and the obtained stereolithography file (STL) was subsequently prepared for printing in Sinterit Studio 2019 1.7.0.1 (Sinterit sp. z o.o., Krakow, Poland) using the process parameters presented in Table S1 – S2. The software allows for set up and adjustment of various parameters including temperatures, model location, and position inside of the chamber (Fig. 1b), layer height as well as laser power ratio (LPR).

There are five parts of which the temperatures can be controlled inside of the printer which are shown in Fig. 2.

The 3D printing process was further carried out as follows: the prepared powder formulations (Table 1) were placed in the powder reservoir (150 × 200 × 150 mm) of the SLS 3D printer (Sinterit Lisa SLS 3D printer, Sinterit, Kraków, Poland). A thin layer of the formulation was thereafter spread onto the build platform after which the powder beds were slowly heated to the temperatures specified in Table S1 – S2. The sintering process was carried out using a 5 W infrared laser diode (λ = 808 nm) in accordance with the template models given in the STL-file in a layer-by-layer fashion. A total of 30 tablets were printed per batch, at a 45° angle to the build platform (i.e. orthogonal to the *x-y* plane, see Fig. 1b), using a layer height of 150 μm. Cylindrical tablets (h = 4 mm, d = 10 mm) were additionally printed at three different angles to the build platform, namely 0°, 45°, and 90° (with respect to the *x-y*-plane, Fig. 1b), in order to evaluate the mechanical properties of the tablets. Specific values for the laser energy transmitted upon the active layer were chosen when printing the different batches. So-called laser power ratio (LPR) is used as a laser power adjustment variable which is defined as a multiplication coefficient of the initial energy output (5 W) and does not have a certain unit. In this study the LPR values 2, 2.5, and 3 were used. The finished batches were retrieved from the build platform at the end of the printing process by sieving. The tablets were additionally de-dusted using pressurized air in order to remove excess powder and stored in sealed containers for further analysis.

2.4. Characterization

Powder X-ray diffraction (PXRD) diffractograms of pristine and heat-treated powder formulations as well as the printed dosage forms were collected on a Bruker D8 Advance TwinTwin diffractometer (Bremen, Germany) using Cu-Kα (λ = 1.5418 Å) radiation. The instrument was operated at 40 mA and 40 kV, using a step-size of 0.02°, and a data collection time of 1 h. Differential scanning calorimetry (DSC)

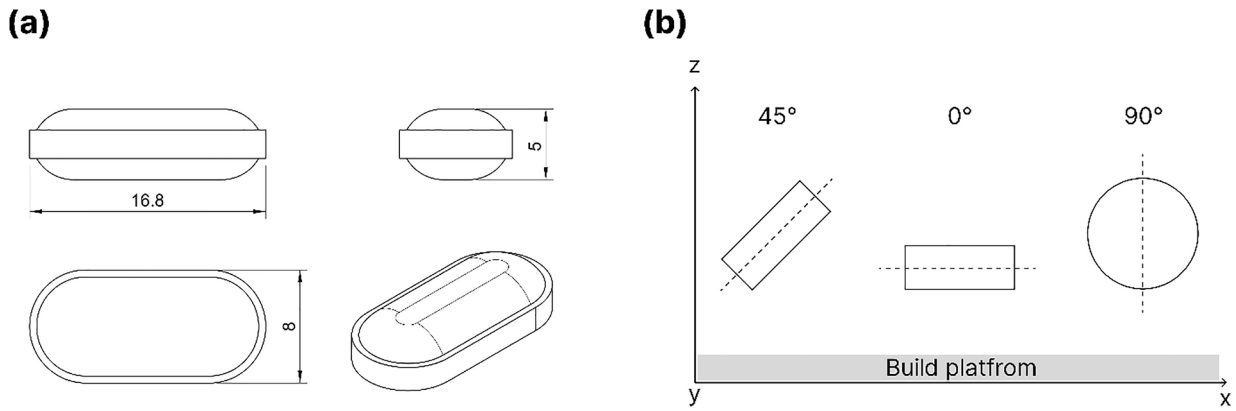

Fig. 1. (a) Orthographic projection and a 3D model of the dosage form, all units are given in mm, and (b)cylindrical tablets orientation scheme with respect to the build platform.

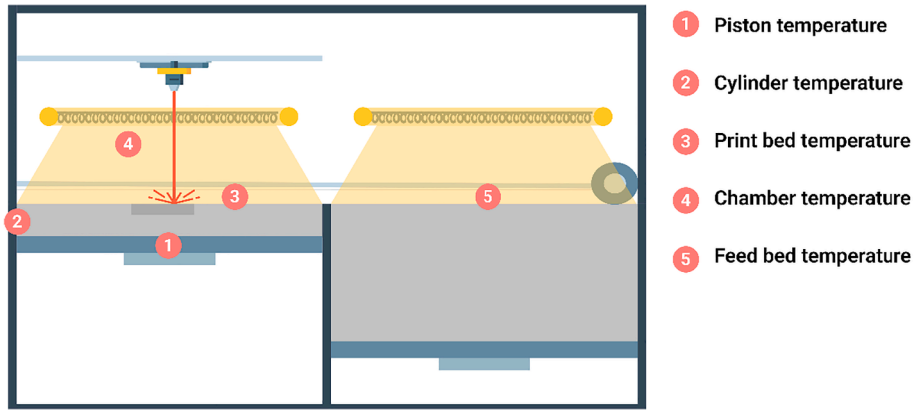

Fig. 2. Schematic drawing of the Sinterit Lisa SLS 3D Printer showing the various temperature elements which may be varied for each printing process.

thermograms were obtained on a Mettler Toledo DSC 3+ (Schwerzenbach, Switzerland) using a heating and cooling rate of 10 °C min^{-1} and nitrogen as purge-gas. Repeated heating–cooling measurements were carried out from −40 to 200 °C and from 200 to 10 °C in the first cycle, and from 10 to 200 °C in the following cycles (presented in Figures S3 and S4). X-ray micro-computed tomography (μCT) was performed on a CT-Alpha (Procon X-Ray, Sarstedt, Germany) with following reconstruction in VG Studio (Volume Graphics D, Germany). The instrument was operated at 80 kV and 30 mA, using a voxelsize of 10 μm and exposure time of 500 ms. A total of 1600 projections were collected for each measured sample and used for the porosity analysis. The porosity of the printed structures was calculated as the ratio between the volume fraction of the pores and the total volume of the printed structure. The Avizo 3D 2022.2 software (Thermo Fisher Scientific Inc., USA) was used for the analysis. The dimensions (n = 10) and weights (n = 30) of the printed tablet were examined using a digital caliper and an analytical balance (Mettler Toledo XS 64 Analytical Balance, Schwerzenbach, Switzerland). Friability tests were carried out in accordance with the European Pharmacopoeia 2.9.7 (Pharmacopoeia, 2020) on approx. 6.5 g of tablets using a Pharmatest PTF E Friabilator (Hainberg, Germany) at 25 rpm and for 100 rotations. The tablets were carefully weighed pre- and post-measurement and the total weight loss of the tablets (i.e., friability) was calculated. Measurements of the breaking force (given in Newtons, N) were obtained from diametrical compression tests carried out on ten cylindrical tablets (10 mm in diameter) from batches printed at different angles to the printing platform. The Pharmatest PTB 311E tablet hardness testing instrument (Hainberg, Germany) was used in the current study.

2.5. *In-vitro dissolution tests of printed tablets*

Dissolution tests were carried out using a Sotax AT7 Smart Dissolution Tester (Aesch, Switzerland) according to USP guidelines (The United States Pharmacopeia and National Formulary USP 37–NF 32, 711 Dissolution, The United States Pharmacopeial Convention, Inc., Rockville, MD, 2014). *In-vitro* drug release profiles for the 3D printed tablets (n = 3) were recorded at pH 7.4 (phosphate buffer, 900 mL) at 37 ± 0.5 °C and 50 rpm using a sinker to weigh down the tablets. The drug concentration in the dissolution media was determined with high performance liquid chromatography (HPLC) (Agilent 1260 Infinity II, Agilent Technologies, Inc., Santa Clara, USA) on 20 μL of pre-filtered media (0.45 μm PTFE filters, VWR International GmbH). The HPLC assays were performed at 25 °C using a mobile phase composition of acetonitrile–Milli-Q water–acetic acid (49.45:9.45:1.10 v.v%). Samples were injected into a Kinetex 5u C8 100A column (150 × 4.6 mm, Phenomenex, Inc. Torrance, CA, USA) at a flow-rate of 1.2 mL min^{-1} and the eluent analyzed spectroscopically at 254 nm.

2.6. *Determination of tablet drug loading*

The drug content uniformity of the 3D printed tablets (n = 5) were evaluated by placing the individually pre-weighed tablets into 100 mL volumetric flasks containing 50 mL Milli-Q water. The tablets were stirred at 37 °C and 500 rpm for 1 h, after which the solutions were diluted with HPLC mobile phase, filtered (0.45 μm PTFE filters, VWR International GmbH) and analyzed using the same HPLC method as specified in *section 2.5.*

2.7. Statistical analysis

Statistical analysis of the weight distributions of the printed tablets were calculated using one-way ANOVA and weight probability density distributions were constructed in RStudio 1.4.1717 (RStudio PBC, Boston, USA).

3. Results and discussion

3.1. Solid state characterization of SLS-printed tablets

The printed dosage forms (Table 1 and Table S1 – S2) were prepared from either placebo formulations containing 0.5 – 1 wt% AC as colorant or from drug-loaded powder mixtures with 10 wt% naproxen as active pharmaceutical ingredient (API), and 1 wt% AC. Previous studies have shown carbon to be a suitable pigment for the fabrication of paracetamol-based printlets (Kulinowski et al., 2021) as well as metronidazole-loaded carbon-reinforced polyamide 12 (PA 12) composite printlets (Kulinowski et al., 2022). Other excipients may also be used as absorbing material in order to provide sufficient thermal energy to sinter various polymers in the presence of NIR/IR lasers. One such example includes the combination of the Kollicoat® IR and an IR-absorbing dye (Lekurwale et al., 2022). Well-sintered tablets with no observable defects were obtained from all prepared powder formulations at LPRs between 2 and 3. As can be seen in Fig. 3, a clear and expected difference in shading could be observed between the different batches containing 0.5 – 1 wt% AC and naproxen. The appearance of the tablets was found to be influenced to a lesser degree by the LPR, especially for batches containing 0.5 wt% carbon. However, minor differences in shading between different LPRs were still observable. Which shows the effects that an increased energy input of the laser may have on the visual appearance of the printed tablets (i.e., darkening of the tablet due to a higher degree of sintering).

The laser properties may be described differently, depending on the printer and the laser system inside. For instance, another frequently used SLS printer, Sintratec Kit, uses a galvo-system, which is defined by the scanning speed. In case of the Sinterit printer used in the current study, the more cryptic term LPR defines the laser energy input. Even though the laser systems are different, the output is the same - an energy density that represents the amount of the energy initially emitted upon the active powder layer. The energy density of the laser beam not only affects the appearance of tablets but the mechanical and dissolution properties, which has been observed in other studies (Madžarević et al., 2021; Thakkar et al., 2021; Mohamed et al., 2020). The selection of suitable printing parameters such as LPR or scanning speed and temperatures depends on the thermal and physical properties of the specific polymers, APIs, and colorants (Madžarević et al., 2021; Thakkar et al., 2021; Schmid and Schmid, 2018).

The crystalline state of the API and polymers in the printed dosage forms was evaluated by PXRD and DSC. Diffractograms of the printed batches containing 1 wt% AC, their corresponding physical mixtures, and the pristine polymer and API are shown in Fig. 4. The diffractograms of the placebo dosage forms can be seen to correspond to that of the pristine polymers with some additional emerging peaks for the PVA-based tablets characteristic to that of crystalline PVA at approximately $2\theta = 11.34^{\circ}$, 16.01°, 19.33°, 19.98°, 22.77°, 27.46°, and 32.33° (Bunn, 1948). No peaks corresponding to the API were observed for either batch of naproxen-loaded tablets, indicating that a majority of the drug in the

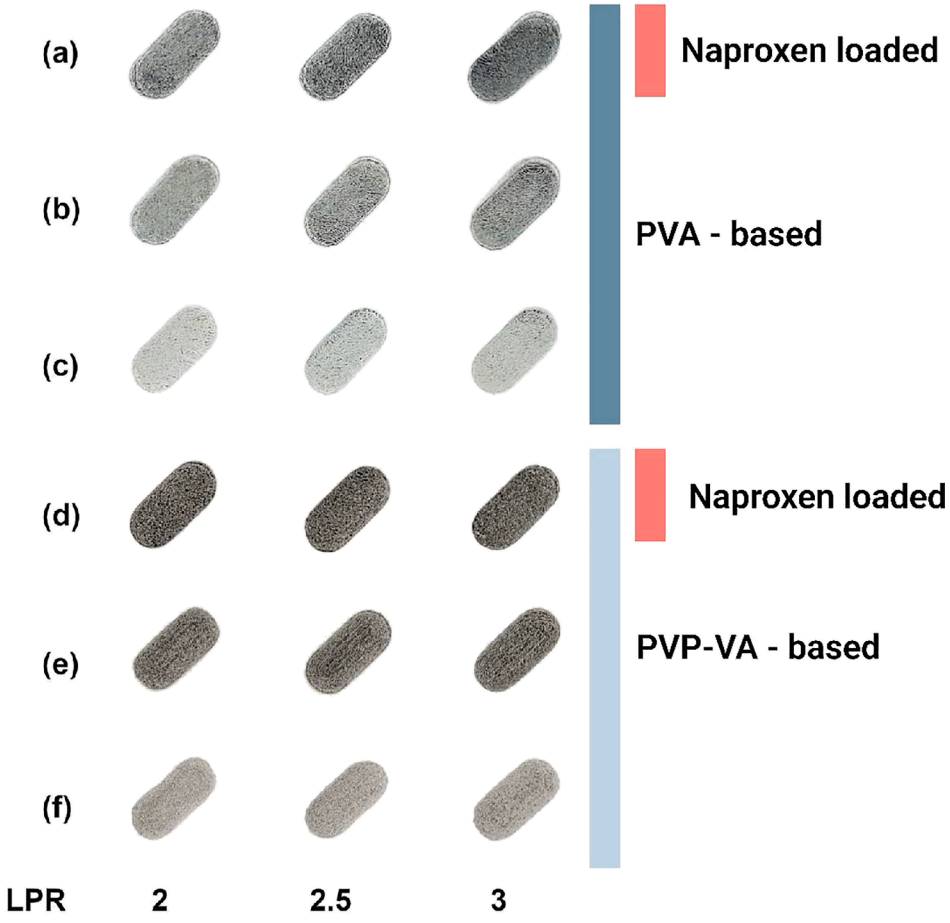

Fig. 3. The camera images of PVA- (a – c) and PVP/VA (d – f) tablets containing (a and d) 10 wt% naproxen and 1 wt% AC, (b and e) 1 wt% AC, and (c and f) 0.5 wt% AC. Images were taken at the same light conditions and camera settings.

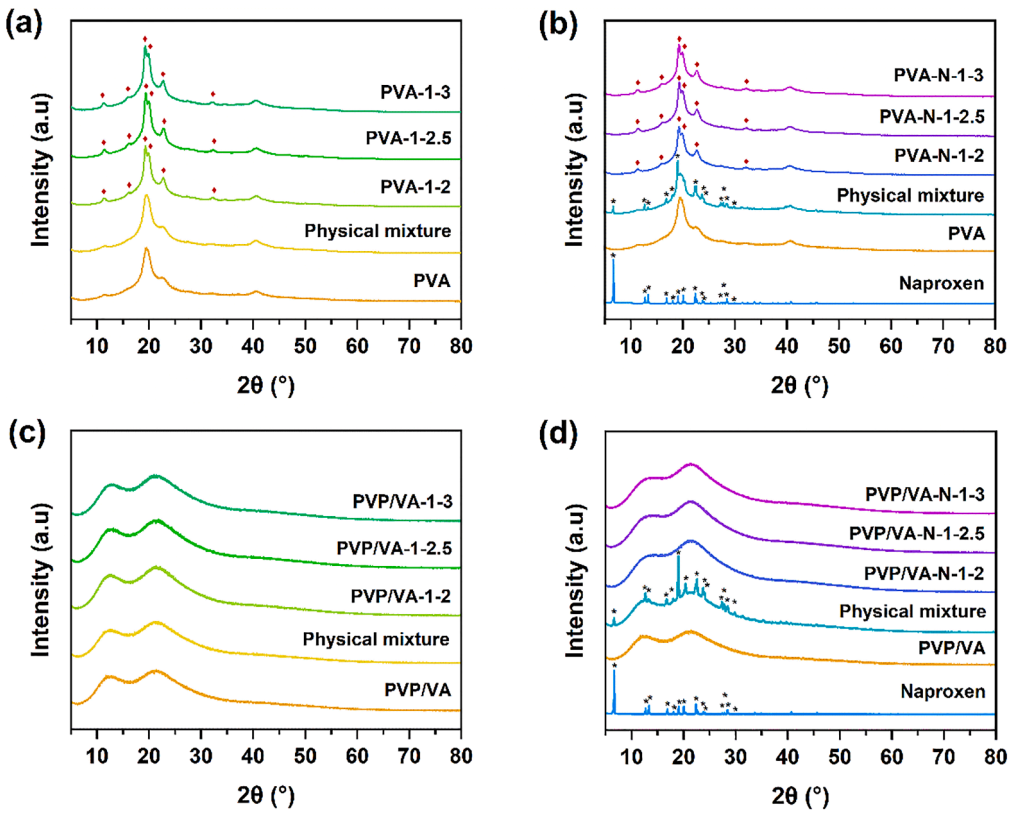

Fig. 4. PXRD diffractograms (λ = 1.5418 Å) of printed placebo and naproxen-loaded solid dosage forms. Phases corresponding to crystalline polyvinyl alcohol and naproxen are highlighted with red diamond symbols and black asterisks, respectively. (For interpretation of the references to colour in this figure legend, the reader is referred to the web version of this article.)

powder formulations was successfully amorphized during the printing process.

DSC thermograms of the printed tablets (Fig. 5) were found to be in good agreement with observations made from the diffractograms. A single glass transition (T_g) event along with an overlapping enthalpy of relaxation peak could be observed for all the PVA-based dosage forms as well as the pristine polymer. Indicating that the API in the naproxen-loaded tablets was molecularly dispersed in the polymer and that an amorphous solid dispersion (ASD) had successfully been obtained (Dedroog et al., 2020). A shift in T_g of approximately 1.5 and 3.5 ℃, as compared to the pristine polymer, was seen for the placebo and naproxen-loaded batches, respectively, further indicating that the colorant and/or API may act as weak plasticizers. The thermograms of the PVP/VA-based dosage forms, on the other hand, showed no discernable glass transition in the measured temperature interval. This was found to be due to the broad endothermic peak at approximately 90 ℃ corresponding to the desorption of water in the polymer in the first heating cycle, which coincides with the reported T_g of PVP/VA (i.e. Plasdone S-630) at 109 ℃ (Bordos et al., 2019). No melting peak corresponding to naproxen at 158.5 ℃ was observed for either drug-loaded batch, confirming the amorphous state of the API in the printed tablets. Notably, such events were also found to be absent in the physical

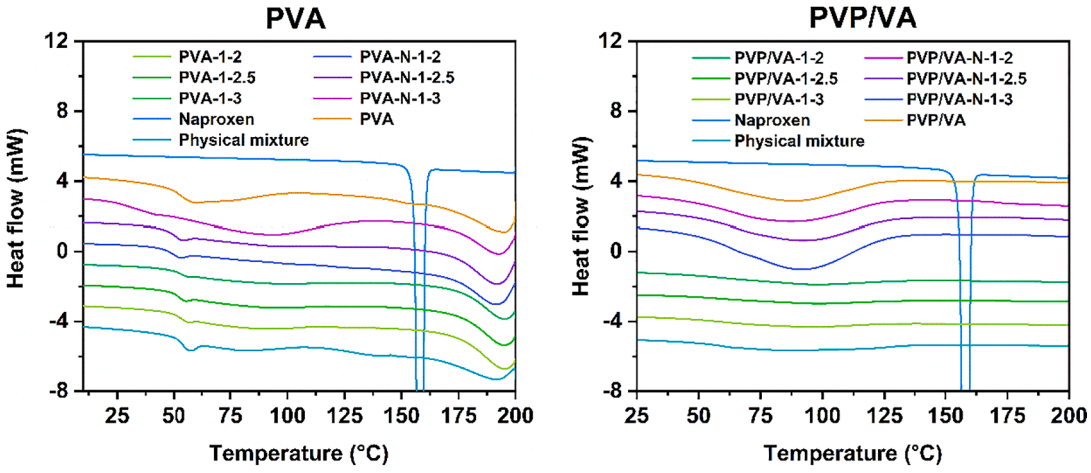

Fig. 5. DSC thermograms of naproxen-loaded and placebo tablets containing 1 wt% AC along with the pristine polymers and API. Presented thermograms represent the first heating cycle.

mixtures. The combination of DSC and PXRD is widely used to identify traces of crystalline material (Dedroog et al., 2020) and is suitable for different types of drugs with different melting peaks, such as Paracetamol (T_m = 172 ℃) (Qi et al., 2008) or Naproxen (T_m = 158.5 ℃), in the current study. In both cases, the melting endotherm in the DSC profile disappears after the sintering process, which is caused by the dissolution of the API into the polymer matrix at the temperature above T_g of the polymer regardless of the melting temperature of the API. This demonstrates that the API was able to dissolve in the polymer matrices below the melting point of the drug, thus showing that ASDs may be formed using either PVA or PVP/VA. In the case of PVP/VA, the dissolution of the API in the polymer likely occurred between 109 and 158 ℃ at the flowing point, T_f, of the polymer (i.e. the temperature at which the polymeric chains gain greater mobility and the polymer enters a viscous liquid state) (Schmid and Schmid, 2018).

3.2. Weight uniformity and tablet dimensions

The recorded mass of the placebo tablets containing 0.5 and 1 wt% AC as well as the naproxen-loaded tablets are presented in Fig. 6, Figure S6, and Table S4 – S5. A significant difference ($P < 0.05$) between the weight distributions of the placebo tablets could be seen. Indicating that the average tablet weight could be effectively controlled by the addition of more colorant. An overlap in the mass distributions could be seen for PVA-05–3 and PVA-1–2 (Fig. 6a) as well as PVP/VA-05–3 and PVP/VA-1–2 (Fig. 6c), i.e., batches printed with the highest and lowest LPR using 0.5 wt% and 1 wt% AC, respectively. Demonstrating that tablets of comparable weight may be obtained at different colorant concentrations by varying the LPR. Comparisons between the naproxen-loaded batches (PVA-N-1) and placebo tablets (PVA-1) containing 1 wt% AC also show that the obtained PVA-based tablets were similar in mass. An increase in average tablet weight by 4.79, 1.66, and 0.63 wt% was observed for the naproxen-loaded batches as compared to the placebo tablets when the LPR was increased. According to the acquired data, the weight and weight distributions depend on the polymer selection even though other concentrations and printing parameters were kept the same. The main reason for this behavior is the thermal properties of polymers, especially T_g. Previous studies have shown a strong correlation between poor printability (insufficient sintering resulting in extremely low tablet weights) and the high value of T_g (Schmid, 2018; Yan et al., 2011; Chatham et al., 2019). Similar trends were however not detected for the PVP/VA-based dosage forms, where significant weight differences between the naproxen-loaded tablets were observed for all batches aside from PVP/VA-N-1–2.5 and PVP/VA-N-1–3. Indicating that smaller increments in LPR and carbon concentration may be required in order to tune the tablet weight in such formulations.

The dimensions of the printed tablets were found to remain consistent across all batches, only increasing slightly with colorant concentration, drug loading, or LPR, especially for the PVP/VA-based tablets (Tables S4 – S5). This indicates that the observed increase in tablet weight was related to a densification of the printed structures and not to an increase of their dimensions. However, it is important to note that small deviations in the tablet volume, which may be too small to accurately measure using a caliper, could contribute significantly. An average deviation of 2.31, 1.53, 0.42 wt% and 3.49, 7.22, 2.19 wt% in the length, height, and width of the PVA- and PVP/VA-based tablets, respectively, were seen as compared to the theoretical model (Fig. 1). Despite the relatively small dimensional variations, the difference is crucial in case of dosage forms printing. Even small deviations might cause an incorrect dose of the API within the printed tablet. The temperature difference and heating/cooling cycling during the printing process are the main reasons for layer warping and shrinkage effects (Schmid, 2018). This issue can be compensated by adding offset values selected according to the formulation content and API concentration. These may be related to additional adhesion of the powder to the printed structures (due to over-sintering) and/or to tablet shrinkage during the

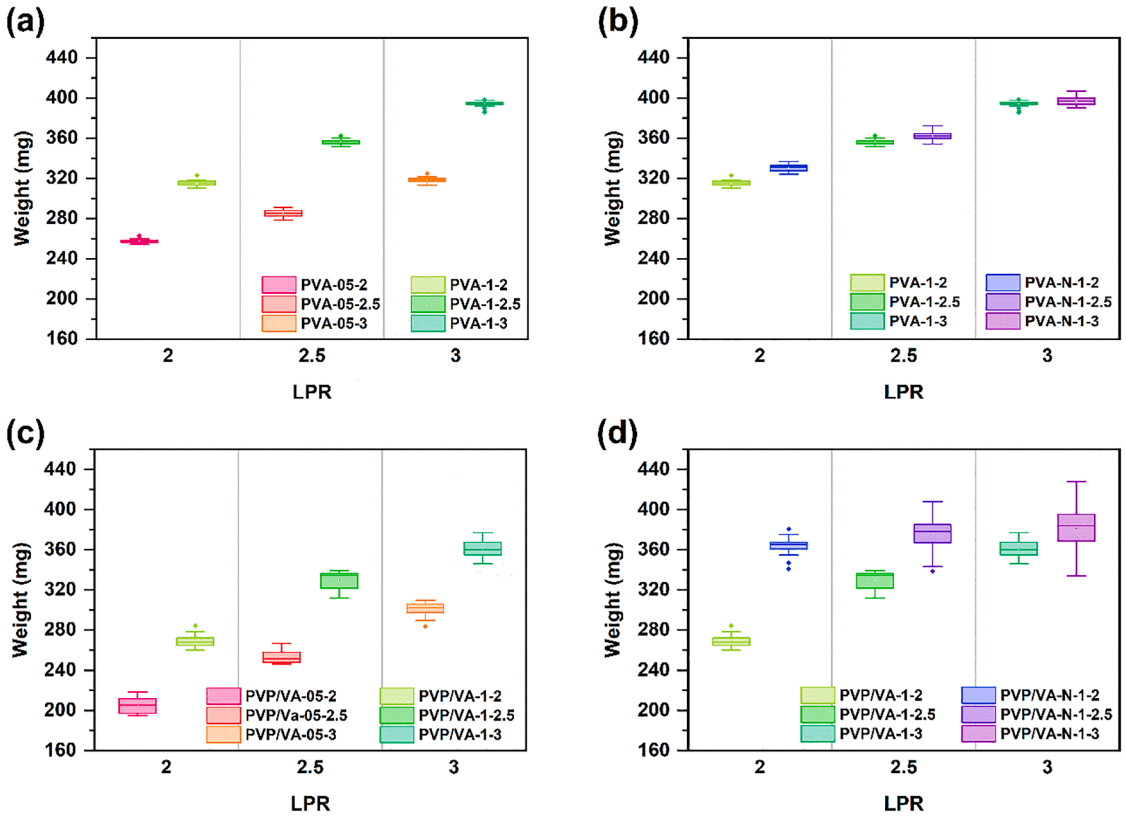

Fig. 6. Box-plots showing the weight distributions of (a) PVA-based placebo tablets containing 0.5 and 1 wt% AC, (b) naproxen-loaded PVA-based tablets containing 1 wt% AC, (c) PVP/VA-based placebo tablets containing 0.5 and 1 wt% AC, and (d) naproxen-loaded PVP/VA-based tablets containing 1 wt% AC.

cooling process (Schmid, 2018).

The recorded friability was found to be < 1 wt% for all but two and four batches of the PVA- and PVP/VA-based dosage forms, respectively. Thus, the majority of the printed tablets were in compliance with the specifications (<1.0 wt% friability) given by the European Pharmacopoeia 2.9.7 – Friability of Uncoated Tablets (Ed. 10.0) (Pharmacopoeia, 2020). The PVA-based placebo tablets containing 0.5 wt% AC and printed at 2 and 2.5 LPR were observed to be insufficiently sintered, resulting in a higher tablet weight loss of 1.31 and 1.11 wt%, respectively (Table S4). Similarly, all PVP/VA-based naproxen-loaded batches and the placebo tablets containing 1 wt% AC printed at an LPR of 3 were observed to be well-sintered, resulting in a tablet weight loss < 0.85 wt% (Table S5). A decreasing trend in friability was also observed with increasing LPR, which was expected due to the densification of the structures arising from a higher degree of sintering (i.e. due to the partial melting and subsequent re-solidification of the polymers/API).

X-ray microtomography (μCT) images of the placebo and naproxen-loaded PVA-based tablets (Fig. 7), show a clear decrease in observable porosity with increasing LPR. The following computation showed that the volume fraction of pores is 21.4% and 13.2% in case of PVA-1–2 and PVA-1–3, respectively. This confirms that the previous observations regarding the increase in tablet weight may indeed be partially explained by a structural densification. However, the pore volume fraction in case of the API-loaded structure (PVA-N-1–3) reached 31.9%. An increase in the porosity is likely caused by the denser API-polymer fusion during the sintering process and its following solidification and shrinkage.

Due to the higher LPR and hence the higher thermal energy absorbed by the powder bed, actual melting of the polymer occurs. The molten polymer fills the voids between the particles and dissolves the API in its matrix, resulting in the formation of cavities (Fig. 8). These cavities follow the shape of the newly printed layer and are filled with additional powder after the fresh layer has been applied. The intralayer porosity can be seen to become less homogenous as the LPR increases. The formation of apparently isolated cavities within the layers, which may arise from incomplete sintering of adjacent lines, is observed. The addition of 10 wt% naproxen to the formulation further amplifies these macroscopic features characterized by a different particle shape (Figure S1) and possibly indicates that the API and/or colorant may be present as smaller aggregates (Table S3). Thus, it may lead to a local variation in degree of sintering within the layer. Changes in the degree of porosity lead to changes in the dissolution behavior due to the close/open access to the dissolution medium (Kulinowski et al., 2021).

The hardness of the PVP/VA-based placebo tablets were further evaluated as a function of printing angle (Fig. 9). A significant difference ($P < 0.05$) in tablet hardness was observed between the tablets printed at 0°, 45°, and 90° to the print plate. Such anisotropic response to mechanical stress has previously been reported for other SLS printed structures and mainly arises from differences in particle sintering within and between each printed layer (i.e., variations in layer adhesion in the *xy*-plane as well as along the *z*-axis) (Cooke et al., 2011). A decrease in hardness could be observed with increasing print angle and was found to be due to the applied mechanical stress aligning with the printed layers. Thus, showing that the inter-layer sintering along the *z*-axis was weaker as compared to the sintering in the *xy*-plane. Further, the hardness of the tablets was also found to be dependent on the carbon concentration and LPR, which was expected due to a higher degree of sintering.

3.3. Drug release

Drug release profiles of the naproxen-loaded tablets in pH 6.8 phosphate buffer (Fig. 10) show that 90% of the drug content was released within 180 min and 60 min for the PVA- and PVP/VA-based tablets, respectively. Even though dissolution appears to be complete after 120 min in case of PVP/VA-based formulations, deviations from the expected release of 100% were observed. Potential reasons might be inhomogeneities in the powder blend or absorption of drug to the polymers. As the focus of this study was a comparison of polymers in SLS, we did not investigate this issue further. Tablets sintered using the lowest and highest LPRs (i.e. PVA-N-1–2, PVA-N-1–3 and PVP/VA-N-1–2, PVP/VA-N-1–3) were observed to have the fastest and slowest drug release rates, respectively. Particularly in the case of the PVA-based tablets, where a 90% drug release was reached within 90 and 180 min, respectively. However, a significant swelling of PVA-based dosage forms was observed within the first two hours because of the low solubility of the polymer in the high pH environment. This caused the variation in cumulative release within triplicates. This feature of PVA is well-known and was described previously in case of FDM printed capsules for drug delivery (Matijašić et al., 2019). Differences in release rate between the batches were however less apparent in the PVP/VA-based tablets, indicating that PVP/VA may be less responsive to changes in LPR as compared to PVA. The dissolution behavior of the printed tablets was found to correspond well with the results obtained from the μCT images regarding the densification of the structures (Fig. 7) with increasing carbon concentration and LPR. This shows that the release rate of the API can be tailored by changing the energy input of the laser during the printing process by producing structures of varying densities. According to recent studies (Kulinowski et al., 2021; Kulinowski et al., 2022), the dissolution profile can vary depending on the sintering degree. In case of a higher amount of heat energy transferred upon the printing layer, the layers interact stronger and voids between powder particles are filled by viscous polymer after passing the T_g-point. In case of high scanning speed and using highly-soluble polymers such as Kollidon 90% of the API can be released within 5 min and disintegration can

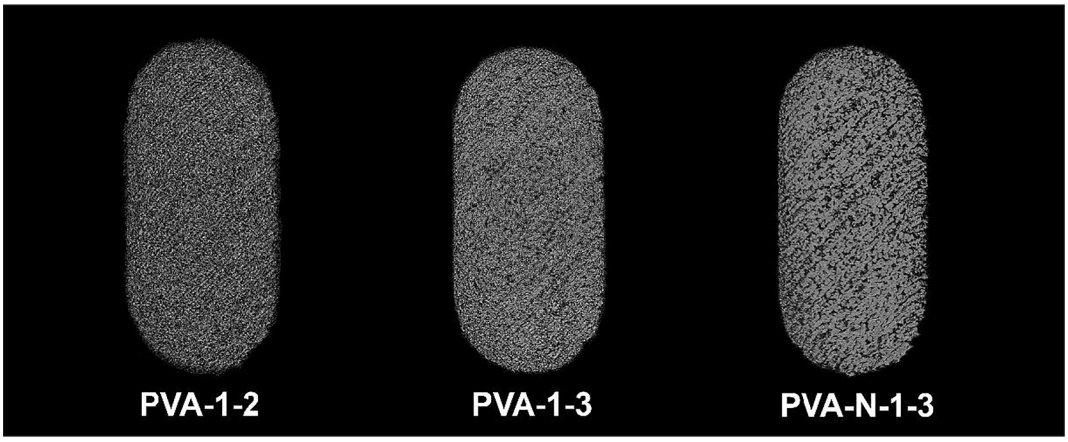

Fig. 7. μCT images of placebo and naproxen-loaded PVA-based tablets containing 1 wt% AC and printed at LPRs of 2 and 3.

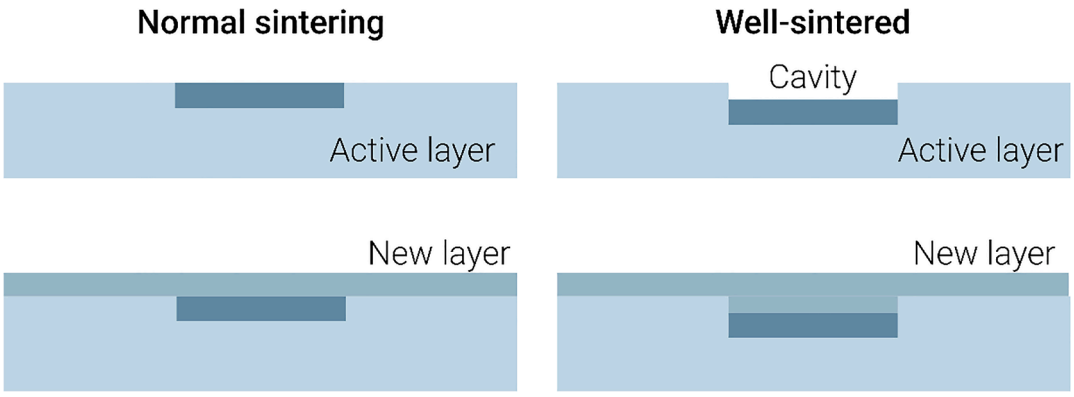

Fig. 8. Cavity formation and following densification process in case of well-sintering.

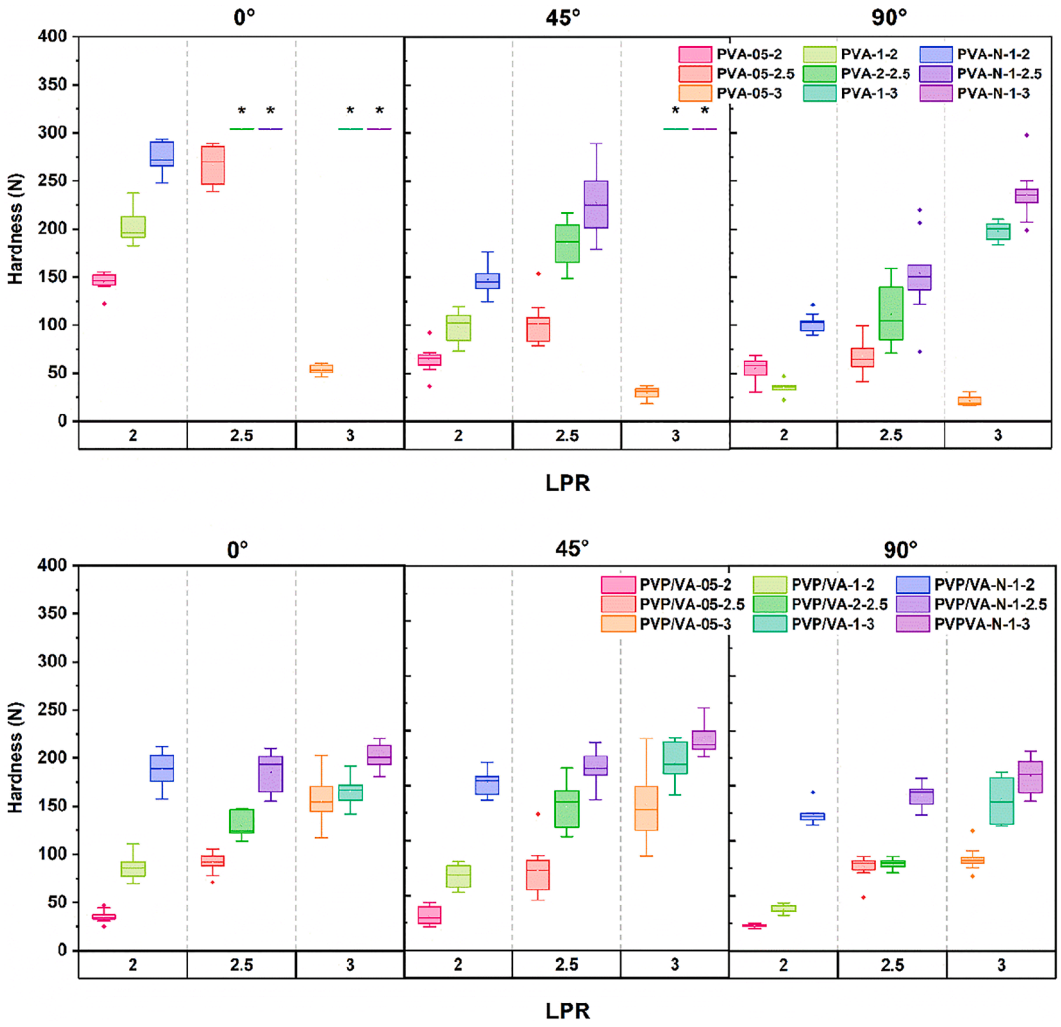

Fig. 9. Boxplots showing the correlation between tablet hardness and printing angle for (a) the PVA-based and (b) PVP/VA-based tablets (n = 12). Tablets exceeding 310 N in hardness are highlighted in the figure with asterisks.

occur within 15 s (Allahham et al., 2020).

The average drug loading of the naproxen-loaded tablets (Table 2) were shown to be slightly lower than the theoretical loading of 10 wt%. Both PVA, PVP/VA, and naproxen were shown to be thermally stable in the temperature range used to print the dosage forms (Figure S5) and no evidence of drug degradation was observed according to HPLC analysis. Thus, the lower drug loading may be related to a loss of the API during the powder preparation process. Deviations in the drug content within each batch was found to be < 0.35 wt% and, thus, the mixing of the powder formulations during the preparation process were assumed to be sufficient.

4. Conclusions

PVA- and PVP/VA-based placebo as well as naproxen-loaded tablets were successfully printed using a selective laser sintering 3D printing

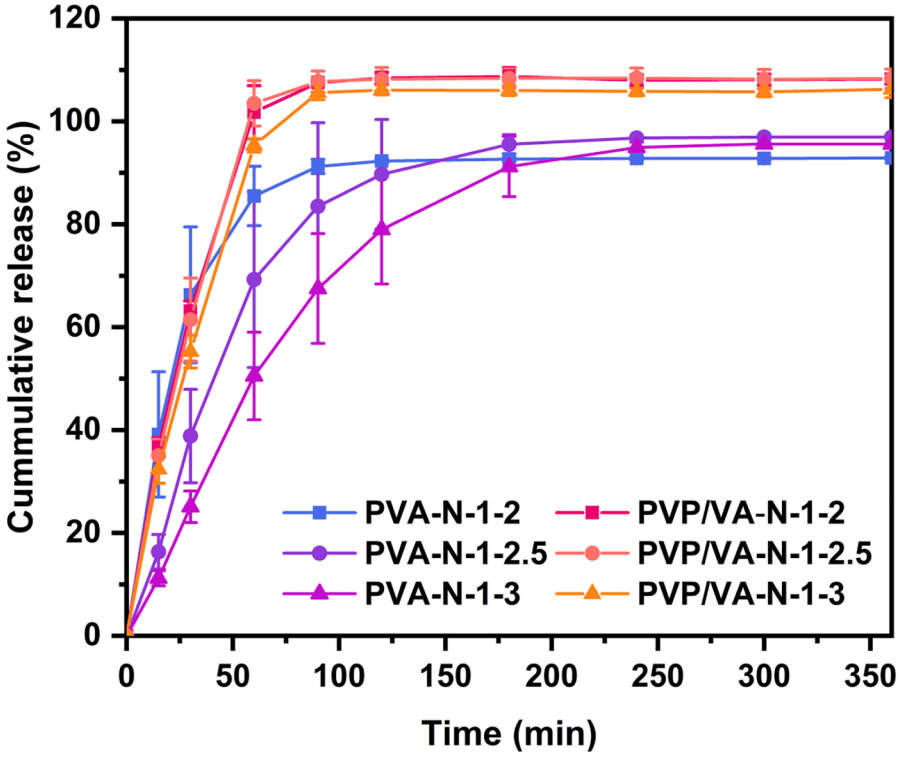

Fig. 10. Drug release profiles of PVA- and PVP/VA-based naproxen-loaded tablets (n = 3) in pH 6.8 phosphate buffer.

Table 2
Average drug loading of naproxen-loaded tablets (n = 5).

Formulation	Drug loading (wt%)	Drug loading (mg per tablet)	Tablet weight (mg)
PVA-N-1–2	9.42 ± 0.12	31.11 ± 0.71	330.29 ± 3.50
PVA-N-1–2.5	9.04 ± 0.22	32.68 ± 0.57	361.41 ± 3.43
PVA-N-1–3	9.08 ± 0.06	36.14 ± 0.27	398.22 ± 2.48
PVP/VA-N-1–2	9.0 ± 0.23	34.18 ± 0.67	379.88 ± 2.47
PVP/VA-N-1–2.5	8.8 ± 0.14	32.83 ± 1.52	375.22 ± 23.31
PVP/VA-N-1–3	8.7 ± 0.34	34.26 ± 1.53	393.32 ± 5.61

technique. The weight and hardness of the printed tablets could be tailored by either changing the laser energy input or the colorant concentration in the formulations. *In-situ* amorphization of the API at 10 wt % loading was achieved during the printing process for both polymers without any observable degradation of the drug. Further, the release rate of the API from the printed structures could be tailored by changing the laser energy input or the colorant concentration in the formulations, producing structures of varying porosities. PVA-based placebo tablets showed better friability results compared to PVP/VA-based, whereas drug-loaded batches have mass losses of<1 wt% for both polymers. However, PVP/VA-based naproxen-loaded tablets have poor mass uniformity which is caused by the higher glass transition point and, consequently, worse polymer/drug interaction during sintering process at the selected printing temperature of 85 C. This study demonstrates that SLS 3D printing may be a promising technique for manufacturing large batches of solid dosage forms from polymers with different physical properties. Nevertheless, many parameters affect the final printed structures, among others, temperature, LPR, concentration of the colorant and API. The effect of each parameter can be estimated empirically and/or in combination with Quality by Design methods. This study shows, as mentioned above, that the LPR or laser sintering speed has the largest impact on the print outcome. Thus, producing tablets with tailorable properties for personalized medicines. Future studies exploring the drug-polymer interactions and drug release behavior of the API-loaded tablets will be crucial in further evaluating this technique.

CRediT authorship contribution statement

Evgenii Tikhomirov: Conceptualization, Methodology, Investigation, Writing – original draft, Visualization. **Michelle Åhlén:** Conceptualization, Methodology, Investigation, Writing – original draft, Visualization. **Nicole Di Gallo:** Methodology, Investigation. **Maria Strømme:** Conceptualization, Writing – review & editing, Supervision, Funding acquisition. **Thomas Kipping:** Conceptualization, Writing – review & editing. **Julian Quodbach:** Conceptualization, Writing – review & editing, Supervision. **Jonas Lindh:** Conceptualization, Writing – review & editing, Supervision, Funding acquisition.

Declaration of Competing Interest

The authors declare the following financial interests/personal relationships which may be considered as potential competing interests: [Jonas Lindh reports financial support was provided by Merck KGaA.].

Data availability

Data will be made available on request.

Acknowledgements

Thanks are due to Kokott Marcel for assistance with the experiments and performing X-ray micro-computed tomography. Many thanks are due to Mark Carroll for performing analysis and volume fraction of pores computation. Funding by Merck KGaA, Germany is gratefully acknowledged. Funding by the Erling-Persson Family Foundation (2017), Sweden is gratefully acknowledged. This work is conducted within the Additive Manufacturing for the Life Sciences Competence Center (AM4Life). The authors gratefully acknowledge financial support from Sweden's Innovation Agency VINNOVA (Grant no: 2019-00029)

Appendix A. Supplementary material

Supplementary data to this article can be found online at https://doi.org/10.1016/j.ijpharm.2023.122780.

References

Allahham, N., Fina, F., Marcuta, C., Kraschew, L., Mohr, W., Gaisford, S., Basit, A.W., Goyanes, A., 2020. Selective laser sintering 3D printing of orally disintegrating printlets containing ondansetron. Pharmaceutics 12, 110. https://doi.org/10.3390/pharmaceutics12020110.

Awad, A., Fina, F., Goyanes, A., Gaisford, S., Basit, A.W., 2020. 3D printing: Principles and pharmaceutical applications of selective laser sintering. Int. J. Pharm. 586, 119594 https://doi.org/10.1016/j.ijpharm.2020.119594.

Awad, A., Fina, F., Goyanes, A., Gaisford, S., Basit, A.W., 2021. Advances in powder bed fusion 3D printing in drug delivery and healthcare. Adv. Drug Deliv. Rev. 174, 406–424. https://doi.org/10.1016/j.addr.2021.04.025.

Bordos, E., Islam, M.T., Florence, A.J., Halbert, G.W., Robertson, J., 2019. Use of terahertz-raman spectroscopy to determine solubility of the crystalline active pharmaceutical ingredient in polymeric matrices during hot melt extrusion. Mol. Pharmaceutics 16, 4361–4371. https://doi.org/10.1021/acs.molpharmaceut.9b00703.

Bunn, C.W., 1948. Crystal structure of polyvinyl alcohol. Nature 161, 929–930. https://doi.org/10.1038/161929a0.

Cailleaux, S., Sanchez-Ballester, N.M., Gueche, Y.A., Bataille, B., Soulairol, I., 2021. Fused deposition modeling (FDM), the new asset for the production of tailored medicines. J. Control Release 330, 821–841. https://doi.org/10.1016/j.jconrel.2020.10.056.

Chang, S.Y., Li, S.W., Kowsari, K., Shetty, A., Sorrells, L., Sen, K., Nagapudi, K., Chaudhuri, B., Ma, A.W.K., 2020. Binder-jet 3D printing of indomethacin-laden pharmaceutical dosage forms. J. Pharm. Sci. 109, 3054–3063. https://doi.org/10.1016/j.xphs.2020.06.027.

Charoo, N.A., Barakh Ali, S.F., Mohamed, E.M., Kuttolamadom, M.A., Ozkan, T., Khan, M.A., Rahman, Z., 2020. Selective laser sintering 3D printing - an overview of the technology and pharmaceutical applications. Drug Dev. Ind. Pharm. 46, 869–877. https://doi.org/10.1080/03639045.2020.1764027.

Chatham, C.A., Long, T.E., Williams, C.B., 2019. A review of the process physics and material screening methods for polymer powder bed fusion additive manufacturing. Prog. Polym. Sci. 93, 68–95. https://doi.org/10.1016/j.progpolymsci.2019.03.003.

Cooke, W., Tomlinson, R.A., Burguete, R., Johns, D., Vanard, G., 2011. Anisotropy, homogeneity and ageing in an SLS polymer. Rapid Prototyp. J. 17, 269–279. https://doi.org/10.1108/13552541111138397.

Davis Jr., D.A., Thakkar, R., Su, Y., Williams 3rd, R.O., Maniruzzaman, M., 2021. Selective laser sintering 3-dimensional printing as a single step process to prepare amorphous solid dispersion dosage forms for improved solubility and dissolution rate. J. Pharm. Sci. 110, 1432–1443. https://doi.org/10.1016/j.xphs.2020.11.012.

Dedroog, S., Pas, T., Vergauwen, B., Huygens, C., Van den Mooter, G., 2020. Solid-state analysis of amorphous solid dispersions: Why DSC and XRPD may not be regarded as stand-alone techniques. J. Pharm. Biomed. Anal. 178, 112937 https://doi.org/10.1016/j.jpba.2019.112937.

El Aita, I., Rahman, J., Breitkreutz, J., Quodbach, J., 2020. 3D-Printing with precise layer-wise dose adjustments for paediatric use via pressure-assisted microsyringe printing. Eur. J. Pharm. Biopharm. 157, 59–65. https://doi.org/10.1016/j.ejpb.2020.09.012.

Fina, F., Goyanes, A., Gaisford, S., Basit, A.W., 2017. Selective laser sintering (SLS) 3D printing of medicines. Int. J. Pharm. 529, 285–293. https://doi.org/10.1016/j.ijpharm.2017.06.082.

Fina, F., Madla, C.M., Goyanes, A., Zhang, J., Gaisford, S., Basit, A.W., 2018. Fabricating 3D printed orally disintegrating printlets using selective laser sintering. Int. J. Pharm. 541, 101–107. https://doi.org/10.1016/j.ijpharm.2018.02.015.

Fina, F., Goyanes, A., Madla, C.M., Awad, A., Trenfield, S.J., Kuek, J.M., Patel, P., Gaisford, S., Basit, A.W., 2018. 3D printing of drug-loaded gyroid lattices using selective laser sintering. Int. J. Pharm. 547, 44–52. https://doi.org/10.1016/j.ijpharm.2018.05.044.

Gueche, Y.A., Sanchez-Ballester, N.M., Bataille, B., Aubert, A., Leclercq, L., Rossi, J.-C., Soulairol, I., 2021. Selective laser sintering of solid oral dosage forms with copovidone and paracetamol using a CO_2 laser. Pharmaceutics 13, 160. https://doi.org/10.3390/pharmaceutics13020160.

Gueche, Y.A., Sanchez-Ballester, N.M., Cailleaux, S., Bataille, B., Soulairol, I., 2021. Selective laser sintering (SLS), a new chapter in the production of solid oral forms (SOFs) by 3D printing. Pharmaceutics 13, pp. https://doi.org/10.3390/pharmaceutics13081212.

Gultekin, H.E., Tort, S., Acarturk, F., 2019. An effective technology for the development of immediate release solid dosage forms containing low-dose drug: Fused deposition modeling 3D printing. Pharm. Res. 36, 128. https://doi.org/10.1007/s11095-019-2655-y.

Hamed, R., Mohamed, E.M., Rahman, Z., Khan, M.A., 2021. 3D-printing of lopinavir printlets by selective laser sintering and quantification of crystalline fraction by XRPD-chemometric models. Int. J. Pharm. 592, 120059 https://doi.org/10.1016/j.ijpharm.2020.120059.

Healy, A.V., Fuenmayor, E., Doran, P., Geever, L.M., Higginbotham, C.L., Lyons, J.G., 2019. Additive manufacturing of personalized pharmaceutical dosage forms via stereolithography. Pharmaceutics 11, pp. https://doi.org/10.3390/pharmaceutics11120645.

Kader, R., Liminga, G., Ljungman, G., Paulsson, M., 2021. Manipulations of oral medications in paediatric neurology and oncology care at a Swedish university hospital: Health professionals' attitudes and sources of information. Pharmaceutics 13, 1676. https://doi.org/10.3390/pharmaceutics13101676.

Kollamaram, G., Croker, D.M., Walker, G.M., Goyanes, A., Basit, A.W., Gaisford, S., 2018. Low temperature fused deposition modeling (FDM) 3D printing of thermolabile drugs. Int. J. Pharm. 545, 144–152. https://doi.org/10.1016/j.ijpharm.2018.04.055.

Konta, A.A., Garcia-Pina, M., Serrano, D.R., 2017. Personalised 3D printed medicines: Which techniques and polymers are more successful? Bioeng. 4, pp. https://doi.org/10.3390/bioengineering4040079.

Kulinowski, P., Malczewski, P., Pesta, E., Łaszcz, M., Mendyk, A., Polak, S., Dorożyński, P., 2021. Selective laser sintering (SLS) technique for pharmaceutical applications—Development of high dose controlled release printlets. Addit. Manuf. 38, pp. https://doi.org/10.1016/j.addma.2020.101761.

Kulinowski, P., Malczewski, P., Łaszcz, M., Baran, E., Milanowski, B., Kuprianowicz, M., Dorożyński, P., 2022. Development of composite, reinforced, highly drug-loaded pharmaceutical printlets manufactured by selective laser sintering-in search of relevant excipients for pharmaceutical 3D printing. Materials 15, 2142. https://doi.org/10.3390/ma15062142.

Lekurwale, S., Karanwad, T., Banerjee, S., 2022. *Selective laser sintering (SLS) of 3D printlets using a 3D printer comprised of IR/red-diode laser*. Ann. 3D Print Med. 6, pp. https://doi.org/10.1016/j.stlm.2022.100054.

Madžarević, M., Medarević, Đ., Pavlović, S., Ivković, B., Đuriš, J., Ibrić, S., 2021. Understanding the effect of energy density and formulation factors on the printability and characteristics of SLS irbesartan tablets-application of the decision tree model. Pharmaceutics 13, 1969. https://doi.org/10.3390/pharmaceutics13111969.

Martinez, P.R., Goyanes, A., Basit, A.W., Gaisford, S., 2018. Influence of geometry on the drug release profiles of stereolithographic (SLA) 3D-printed tablets. AAPS PharmSciTech 19, 3355–3361. https://doi.org/10.1208/s12249-018-1075-3.

Matijašić, G., Gretić, M., Vinčić, J., Poropat, A., Cuculić, L., Rahelić, T., 2019. Design and 3D printing of multi-compartmental PVA capsules for drug delivery. J. Drug Delivery Sci. Technol. 52, 677–686. https://doi.org/10.1016/j.jddst.2019.05.037.

Mohamed, E.M., Barakh Ali, S.F., Rahman, Z., Dharani, S., Ozkan, T., Kuttolamadom, M. A., Khan, M.A., 2020. Formulation optimization of selective laser sintering 3D-printed tablets of clindamycin palmitate hydrochloride by response surface methodology. AAPS PharmSciTech 21, 232. https://doi.org/10.1208/s12249-020-01775-0.

European Pharmacopoeia 10th ed., 2.9.7. Friability of Uncoated Tablets, Strasbourg, 2020, pp. 336-337.

Qi, S., Gryczke, A., Belton, P., Craig, D.Q.M., 2008. Characterisation of solid dispersions of paracetamol and EUDRAGIT® prepared by hot-melt extrusion using thermal, microthermal and spectroscopic analysis. Int. J. Pharm. 354, 158–167. https://doi.org/10.1016/j.ijpharm.2007.11.048.

Santitewagun, S., Thakkar, R., Zeitler, J.A., Maniruzzaman, M., 2022. Detecting crystallinity using terahertz spectroscopy in 3D printed amorphous solid dispersions. Mol. Pharm. 19, 2380–2389. https://doi.org/10.1021/acs.molpharmaceut.2c00163.

Schmid, M., 2018. Laser sintering with plastics: Technology, processes, and materials, 1st ed. Hanser, Munich.

Schmid, M., 2018. LS materials: Polymer properties. In: Schmid, M. (Ed.), Laser sintering with plastics: Technology, processes, and materials. Hanser, Munich, pp. 65–99.

Sen, K., Mehta, T., Sansare, S., Sharifi, L., Ma, A.W.K., Chaudhuri, B., 2021. Pharmaceutical applications of powder-based binder jet 3D printing process - A review. Adv. Drug Deliv. Rev. 177, 113943 https://doi.org/10.1016/j.addr.2021.113943.

Seoane-Viano, I., Trenfield, S.J., Basit, A.W., Goyanes, A., 2021. Translating 3D printed pharmaceuticals: From hype to real-world clinical applications. Adv. Drug Deliv. Rev. 174, 553–575. https://doi.org/10.1016/j.addr.2021.05.003.

Thakkar, R., Davis Jr., D.A., Williams 3rd, R.O., Maniruzzaman, M., 2021. Selective laser sintering of a photosensitive drug: Impact of processing and formulation parameters on degradation, solid state, and quality of 3D-printed dosage forms. Mol. Pharm. 18, 3894–3908. https://doi.org/10.1021/acs.molpharmaceut.1c00557.

Thakkar, R., Jara, M.O., Swinnea, S., Pillai, A.R., Maniruzzaman, M., 2021. Impact of laser speed and drug particle size on selective laser sintering 3D printing of amorphous solid dispersions. Pharmaceutics 13, pp. https://doi.org/10.3390/pharmaceutics13081149.

The United States Pharmacopeia and National Formulary USP 37–NF 32, <711> Dissolution, The United States Pharmacopeial Convention, Inc., Rockville, MD, 2014.

Trenfield, S.J., Awad, A., Goyanes, A., Gaisford, S., Basit, A.W., 2018. 3D printing pharmaceuticals: Drug development to frontline care. Trends Pharmacol. Sci. 39, 440–451. https://doi.org/10.1016/j.tips.2018.02.006.

Trenfield, S.J., Tan, H.X., Goyanes, A., Wilsdon, D., Rowland, M., Gaisford, S., Basit, A. W., 2020. Non-destructive dose verification of two drugs within 3D printed polyprintlets. Int. J. Pharm. 577, 119066 https://doi.org/10.1016/j.ijpharm.2020.119066.

Trenfield, S.J., Januskaite, P., Goyanes, A., Wilsdon, D., Rowland, M., Gaisford, S., Basit, A.W., 2022. Prediction of solid-state form of SLS 3D printed medicines using NIR and Raman spectroscopy. Pharmaceutics 14, 589. https://doi.org/10.3390/pharmaceutics14030589.

van der Vossen, A.C., Al-Hassany, L., Buljac, S., Brugma, J.-D., Vulto, A.G., Hanff, L.M., 2019. Manipulation of oral medication for children by parents and nurses occurs

frequently and is often not supported by instructions. Acta Paediatr 108, 1475–1481. https://doi.org/10.1111/apa.14718.

Wang, J., Goyanes, A., Gaisford, S., Basit, A.W., 2016. Stereolithographic (SLA) 3D printing of oral modified-release dosage forms. Int. J. Pharm. 503, 207–212. https://doi.org/10.1016/j.ijpharm.2016.03.016.

Yan, C., Shi, Y., Hao, L., 2011. Investigation into the differences in the selective laser sintering between amorphous and semi-crystalline polymers. Int. Polym. Process. 26, 416–423. https://doi.org/10.3139/217.2452.